PCCP

Electrolyte clusters as hydrogen Sponges: Diffusion Monte Carlo Simulations.

Journal:	*Physical Chemistry Chemical Physics*
Manuscript ID	CP-ART-08-2022-003658.R1
Article Type:	Paper
Date Submitted by the Author:	11-Oct-2022
Complete List of Authors:	Curotto, Emanuele; University of Arcadia, Chemistry & Physics Zane, Amanda; Arcadia University,

PCCP

ARTICLE TYPE

Cite this: DOI: 00.0000/xxxxxxxxxx

Electrolyte clusters as hydrogen Sponges: Diffusion Monte Carlo Simulations.

A.R. Zane, and E. Curotto[a]

Received Date
Accepted Date

DOI: 00.0000/xxxxxxxxxx

We carry out Diffusion Monte Carlo simulations of up to five hydrogen molecules aggregated with two Stockmayer clusters that solvate a single lithium ion. The first one contains six point dipole solvent particles with parameters tuned to emulate nitromethane. The second cluster is a relative large system investigated recently [G. DiEmma, S. Kalette, and E. Curotto, Chem. Phys. Lett. 725 (2019). 80–86]. In both cases we find that the aggregated hydrogen molecules perturb significantly the ground state of the host cluster and form a distorted tetrahedral cage around the Li^+ ion. The fifth hydrogen molecule is absorbed by the larger Stockmayer cluster while remaining in the proximity of the solvated charge.

1 Introduction

Scientific and technological advances in storing and transporting hydrogen,[1] can drastically reduce the infrastructure costs needed to build a hydrogen economy, even if not meeting the benchmarks set forth by the U.S. Department of Energy for the transportation industry.[2] Therefore, finding novel ways of storing hydrogen to create a high energy to mass ratio composition comparable to fossil fuels remains an active area of applied and fundamental research.[3–8] Current research focuses mostly on chemisorbed hydrogen in the form of hydrides, caged into either Metal Organic Frameworks (MOF)s,[4,6–10] chlathrates, or else adsorbed by various porous surfaces.[5]

For physisorbed hydrogen, some fundamental physics considerations guide the search for good candidates as potential carrier materials. The hydrogen molecule has a vanishing dipole, it is not very polarizable, and because of its small size, is attracted only weakly by dispersion forces. Perhaps the strongest binding occurs when the carrier material, though neutral overall, is in a configuration that displaces charges by distances significantly greater than the size of hydrogen.

Frozen solutions of ionic compounds or frozen ionic liquids may provide a new venue of exploration for potential hydrogen storage solutions. Unlike the charged corner as a model for a type of isoreticular MOFs,[11] frozen solutions of ionic materials may provide a variety of configurations that can be more conducive to the binding of multiple molecules of hydrogen around point charges. Clearly, no single investigation, no matter how broad in scope,[4] can encompass the vast amount of possibilities for composition and configurations of the matter carrier.

In particular, we consider the possibility of modeling amorphous frozen electrolytes surfaces, or alternatively fine powders of these as hydrogen carriers.[12–14] The long term plan is to use clusters as models for such amorphous materials. This approach allows one to create multiple replicas of adsorption sites with different distorted structures and provide a more realistic picture of the structure–property relations that may lead to a rational design approach.[15–18] In the case of charged clusters, it is also possible to gather information by means of hole-burning tagging techniques.[19,20]

One needs only consider the extensive exploration of small to medium sized Lennard Jones clusters published to date,[21–23] to come to the realization that, by itself, the characterization of Electrolyte Clusters (ECs) remains in its infancy.[24–28] The cited works on Lennard Jones aggregates,[21–23] are only a small set of the vast literature, reflecting the complexity of the landscape described with just three parameter, if we include the number of aggregated particles as a degree of freedom. The systematic exploration of the parameter space of clusters of electrolytes, even with the simplest of mathematical models, is likely to require orders of magnitude more effort. Charge solvation, inclusion, segregation, and pairing are all important structural, dynamic and equilibrium features, likely to impact hydrogen storage properties significantly. Moreover, computer simulations of hydrogen storage with any type of substrate can be very insightful only if quantum simulation tools such as Diffusion Monte Carlo,[29–32] are used to handle significant nuclear quantum effects produced by the relatively small mass of the hydrogen molecule.[33–35] Much of our recent development of theoretical and computational tools has been fo-

[a] Department of Chemistry & Physics Arcadia University, 450 S. Easton Rd. Glenside PA E-mail: curotto@arcadia.edu

† Electronic Supplementary Information (ESI) available: [details of any supplementary information available should be included here]. See DOI: 10.1039/cXCP00000x/

cused on improving quantum simulations of structured particles such as point dipoles in the Stockmayer model[36] and the rigid hydrogen.[11,34,35,37–48] Therefore, we feel compelled to begin this journey of exploration in earnest.

In recent investigations, the structure, classical thermodynamics, and ground state properties of ECs comprised of a lithium ion surrounded by points dipoles, are determined.[26–28] The largest of the systems investigated (EC106) is a mixture of two types of Stockmayer particles with parameters matching nitromethane (NM), for six and tetrahydrofuran (THF) for the remaining one hundred components.[26] The global minimum of EC106 features the charge on the surface surrounded by five NM dipoles segregated from the rest, wheareas Li^+ is between two solvation layers in the molten state. The solvated Li^+ has some unusual features. Unlike the octahedral first solvation layer found in small homogeneous Li^+-NM aggregates, only five NM dipoles surround the ion in a slightly distorted square pyramidal shape, with the lithium ion in the center of the base. The vertex of the pyramid is oriented toward the bulk. This particular configuration, stable thanks to the NM - THF interactions, is radically different from typical solvated charge system, leaving a relatively large amount of room around the ion. Therefore, the site's ability to bind multiple hydrogen molecules deserves a closer look. In the simulations of the charged corner model[11] we find that only one H_2 is in the proximity of the charge and more strongly bound than the rest of the molecules. A distinct nodal region in the wavefunction between the bound molecule and the rest of the hydrogen nanodroplet is observed. We anticipate very different structural and energetic features for the aggregated hydrogen given the unique configurations of the two ECs.

The focus of this article is to determine the energy and structures of hydrogen molecules as they aggregate with two of the recently explored ECs,[26–28] the larger system EC106 mentioned earlier, and EC6, a Li^+ ion surrounded by six NM point dipoles. The smaller EC6-$(H_2)_x$ complexes are chosen for comparison, to verify the generality of the features we observe with hydrogen aggregated to EC106, and to obtain resolution on the sequential biding energy of hydrogen to ECs.

In section 2 we present the details of the potential energy model and the simulation strategy used to estimate the ground state properties of the systems. All our data is in section 3. Our conclusions are in section 4.

2 Methods

2.1 The coordinate map

Each point dipole and rigid hydrogen molecule requires a total of five degrees of freedom, three to locate the center of mass, and two for the orientation relative to the space-fixed frame. The orientations are necessary for H_2 as well, since the interactions are strongly anisotropic. We choose to represent all orientations with stereographic projections, since these have distinct advantages over angular degrees of freedom in DMC simulations.[49,50] For completeness we include their definition.

The map between the Cartesian coordinates of the set of points on the unit sphere,

$$\left\{x,y,x\middle|x^2+y^2+z^2=1\right\}, \tag{1}$$

and their stereographic projections $\{\xi^\mu\}_{\mu=1}^2$ is a set of three equations,

$$x^\mu=\frac{4\xi^\mu}{\sigma+4}, \qquad z=\frac{\sigma-4}{\sigma+4}, \tag{2}$$

where x^μ for $\mu=1$ is the x coordinate and for $\mu=2$ the y coordinate. The sum of the squares of the two projections $\sigma=\delta_{\mu\nu}\xi^\mu\xi^\nu$ is a useful shorthand for what follows. We use Einstein's sum convention throughout, and $\delta_{\mu\nu}$ is Kroneker's delta. The metric tensor is diagonal, and for each linear rigid body it has three eigenvalues corresponding to the total mass of the particle m_t, and two additional entries for each stereographic projection,

$$g_{\mu\nu}=\frac{16I_{\mu\nu}}{(\sigma+4)^2}. \tag{3}$$

The lithium ion block has three values along the main diagonal all equal to the mass of ^{7}Li. $I_{\mu\nu}$ are values of the moment of inertia for each linear object. The values of all m_t and moment of inertia components (diagonal) for each type of point dipole particle are in table 1

Table 1 Masses and moments of Inertia for Nitromethane (NM), Tetrahydrofuran (THF), hydrogen and lithium

Symbol	Species	Values (a.u)
m_t	NM	111152
I_{xx}	NM	308397
I_{yy}	NM	555723
m_t	THF	131267
I_{xx}	THF	466696
I_{yy}	THF	849659
m_t	H_2	3672
$I_{xx}=I_{yy}$	H_2	918
m_t	$^7Li^+$	12781

2.2 Diffusion Monte Carlo

We run all our simulations[29,30] using a second order branching approach,[50] and a time interval Δt of 50.0 a.u. A target population of 10^4 replicas is used for the smaller systems, whereas we use both 10^4 replicas and 10^5 replicas for the larger ones. To simulate EC6-$(H_2)_x$ clusters, we need approximately 1 000 moves to reach equilibrium, and the energy data is collected from an additional 12 000 moves. The entire process is repeated 21 independent times to estimate the statistical fluctuations of the energy. For the EC106-$(H_2)_x$ clusters, each system is first equilibrated with a total of 1.2 million steps, followed by data collection from 100 independent walks each 24 000 steps in size. The large number of independent walks is used to monitor the reproducibility of the energy and the wavefunction, and to estimate the ergodic measure for wavefunctions using a recently developed approach.[51,52]

The metric tensor for a n_D dipoles EC + $(H_2)_n$ is stored in a $n_t=5(n+n_D)+3$ vector $\mathscr{G}_\mu$, whose entries are the effective masses for each of the n_t degrees of freedom. n_D is 106 for EC106 and 6 for EC6. Notably, the effective masses associated with orientation

degrees of freedom, $\mathscr{G}_\mu$, are not uniform. [c.f. eq. (3)]. The update for each degree of freedom q^μ, is

$$q^\mu_{k+1} = q^\mu_k + \eta_k \left(\frac{\Delta t}{\mathscr{G}_\mu} \right)^{1/2}, \tag{4}$$

where η_k is a Gaussian random number with zero mean and unit variance. We make no use of guiding functions in any of our DMC simulations. Therefore, the isotopomers simulated with EC in this study approximate p-H_2. Finally, we run simulations with all the degrees of freedom of EC along with the hydrogen molecules, since we find significant differences in the ground state energy and distributions if the ECs are treated as a single rigid body.

2.3 The potential energy model and its characterization

There are three main contributions to the overall Potential Energy Surface (PES)

$$V = V_{\mathrm{EC}} + V_{\mathrm{H_2-EC}} + V_{\mathrm{H_2-H_2}} \tag{5}$$

The hydrogen - hydrogen PES ($V_{\mathrm{H_2-H_2}}$) is the 4D surface[53] of Patkowski et. al. The potential energy surface of the EC is computed as a sum over all particle pairs. Point dipoles interact via the Stockmayer potential,[26] which contains two terms. The first is the dipole - dipole interaction,

$$V^{(\mathrm{DD})} = \sum_{\{ij\}} \mu_i^{(\mathrm{D})} \mu_j^{(\mathrm{D})} \left[\frac{\mathbf{e}_i \cdot \mathbf{e}_j}{r_{ij}^3} - 3 \frac{(\mathbf{r}_{ij} \cdot \mathbf{e}_i)(\mathbf{r}_{ij} \cdot \mathbf{e}_j)}{r_{ij}^5} \right], \tag{6}$$

where the sum runs over all values of i and j from one to n_D. The second term is the Lennard Jones interaction summed over the same set.

$$V^{(\mathrm{LJ})} = \sum_{\{ij\}} 4\varepsilon_{ij} \left[\left(\frac{r_{ij}^{(0)}}{r_{ij}} \right)^{12} - \left(\frac{r_{ij}^{(0)}}{r_{ij}} \right)^{6} \right]. \tag{7}$$

In eqs. (6) and (7), the vector $\mathbf{r}_{ij} = \mathbf{r}_i - \mathbf{r}_j$ is defined by the Cartesian coordinates of the centers of dipole i and j, and r_{ij} its size. The orientation vector for dipole particle i, $\mathbf{e}_i$ is computed using the definitions of the three Cartesian coordinates $\mathbf{e}_i = (x_i, y_i, z_i)$ in eq. (2).

The final terms of V_{EC} are the charge - dipole interactions

$$V^{\mathrm{qD}} = \sum_{i=1}^{n} q_j \mu_i^{(\mathrm{D})} \frac{\mathbf{r}_j \cdot \mathbf{e}_i}{r_{ij}^3}, \tag{8}$$

where the charge q_j is 1 a.u., $\mathbf{r}_{ij} = \mathbf{r}_i - \mathbf{r}_j$ and $\mathbf{r}_j$ is the location of the lithium ion. The sum of $V^{(\mathrm{DD})}$ in eq. (6), $V^{(\mathrm{LJ})}$ in eq. (7) with a sum over all dipoles - Li^+ pairs included, and V^{qD} in eq. (8) equals V_{EC} in eq. (5). The parameters for these equations have been published in previous work, but are reproduced in table 2 for convenience. The parameters pertaining to each point dipole particle are labeled the same way as in table 1. When computing $V^{(\mathrm{LJ})}$ among different types of particles, a and b, the Lorentz - Berthelot combination rules are used: $\varepsilon_{ab} = (\varepsilon_a \varepsilon_b)^{1/2}$, $r_{ab}^{(0)} = \left(r_a^{(0)} + r_b^{(0)} \right)/2$.

The H_2 - EC interaction, $V_{\mathrm{H_2-EC}}$ is constructed by using a point charge distribution on the hydrogen molecule to reproduce the experimental quadrupole moment. A q_H charge is placed on each of the nuclei and a $-2q_H$ charge is in the center of mass of the molecule. Each of the point charges interact with all the dipoles by means of eq. (8) and with the Li^+ via the Coulomb potential. Furthermore, each H_2 molecule interacts with all the components of EC with Lennard Jones terms computed with eq. (7) using the center of H_2 as the source. The parameters of the Lennard Jones terms and q_H are in table 3. The Lennard Jones parameters are estimates based on the size and classical binding of the hydrogen dimer, combined with the Lorentz-Berthelot rules. Although the solvent scaffold interactions are handled with a coarse grained model, the PES is accurate for the most important interactions. Namely, the cation - H_2 and the H_2-H_2 potentials are atomistic and quite accurate. The surface of Patkwski et. al., in particular, is of spectroscopic quality, whereas the Li^+-H_2 dimer energy at the configuration of the minimum of EC6-H_2 is about 200 cm^{-1} deeper than the F12-MP2 energy computed with a QZ basis set.[54–58]

To characterize the PES for EC106-$(H_2)_x$, we search for the most important minima of each system using a population of replicas obtained at the end of several DMC walks. We select approximately 2×10^5 initial points for a particle swarm optimization of the potential energy. The resulting minima are sorted to select the most important configurations, about 1×10^4 for each system, for further refinement. EC106 is a rigid entity during the particle swarm step to expedite the search. The refinement takes place using the Powell algorithm without constraining any degree of freedom. For the smaller system we use Powell to quench the energy of approximately 1×10^4 configurations selected randomly from an equilibrated DMC simulation.

Table 2 Parameters of $V_{\mathbf{EC}}$

Symbol	Species	Values (a.u.)
$\mu^{(\mathrm{D})}$	NM	1.404
$r^{(0)}$	NM	8.2146
ε	NM	9.196×10^{-4}
$\mu^{(\mathrm{D})}$	THF	0.641
$r^{(0)}$	THF	9.1765
ε	THF	1.2775×10^{-3}
$r^{(0)}$	Li^+	5.20
ε	Li^+	5.69×10^{-4}

Table 3 Parameters of $V_{\mathbf{H_2-EC}}$

Symbol	Species	Values (a.u.)
$r_{(0)}$	NM	4.8078
ε	NM	4.892×10^{-4}
$r_{(0)}$	THF	5.28875
ε	THF	5.766×10^{-4}
$r_{(0)}$	Li^+	3.3005
ε	Li^+	3.848×10^{-4}
q_H	—	0.466168

3 Results

3.1 EC6-$(H_2)_x$

A graphical representation of the global minimum of EC6-$(H_2)_5$ is in Fig. 1. The blue spheres are the NM dipoles arranged as an octahedral cage around the lithium ion (red sphere). The latter is also in the center of a distorted tetrahedron composed of four hydrogen molecules whose centers are represented by white spheres. The building pattern for EC6-$(H_2)_x$ begins with the interstitial hydrogen molecules, up to the completion of the tetrahedral cage when $x = 4$. The fifth hydrogen molecule is in the proximity of one of the edges between two nitromethane - like particles. Some of the higher energy minima of EC6-$(H_2)_5$ have the fifth hydrogen molecule coordinating an edge between blue spheres that is closed to an interstitial H_2, making it an energetically less favourable binding site. In the global minimum, the average distance between Li^+ and the dipoles is 6.4 bohr, whereas the four hydrogen molecules in the interstitial layer are 3.3 bohr away from the Li^+ ion.

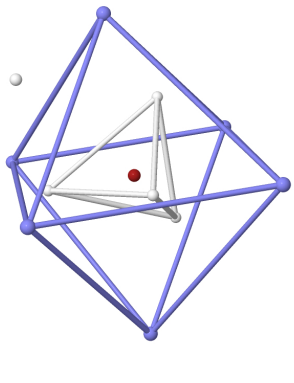

Fig. 1 The interpenetrating global minimum configuration of EC6-$(H_2)_5$. The blue spheres are at the centers of nitromethane - like particles, the white ones at the center of the hydrogen molecules. The lithium ion is the red sphere.

Table 4 Energies of EC6-$(H_2)_x$

cluster	E_0 (hartree)	$V_{\min}$ (hartree)	ZPE (hartree)	μ_x cm^{-1}	$\mu_x^{(c)}$ (cm^{-1})
EC6	-0.15154	-0.1563046	0.00477	-	-
EC6-H_2	-0.15847	-0.1691229	0.01065	1520	2813
EC6-$(H_2)_2$	-0.16534	-0.1819772	0.01664	1510	2821
EC6-$(H_2)_3$	-0.17188	-0.1944223	0.02255	1430	2731
EC6-$(H_2)_4$	-0.17565	-0.2042648	0.02861	829	2160
EC6-$(H_2)_5$	-0.17648	-0.2067673	0.03029	180	549

The classical and ground state energies of the EC6-$(H_2)_x$, $(0 \le x \le 5)$ are in table 4. Column 2 of table 4 contains the values of the ground state energy, E_0, for the six clusters, including the bare EC6, whereas $V_{\min}$ in column 3 is the potential energy value of the global minima. The Zero Point Energy (ZPE) is estimated with $E_0 - V_{\min}$. Columns 5 and 6 contain the quantum and classical chemical potential for the hydrogen molecule respectively, namely,

$$\mu_x = E_0\,(\text{EC6-}(H_2)_x) - E_0\,(\text{EC6-}(H_2)_{x-1})\,, \qquad (9)$$

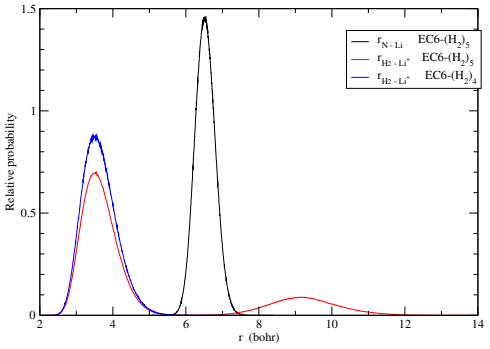

Fig. 2 Selected radial distributions for EC6-$(H_2)_4$ and EC6-$(H_2)_5$.

$$\mu_x^{(c)} = V_{\min}\,(\text{EC6-}(H_2)_x) - V_{\min}\,(\text{EC6-}(H_2)_{x-1})\,. \qquad (10)$$

Therefore, the binding of each H_2 for the first three molecules is about 1500 wavenumbers, a considerably larger value compared to those found in previous investigations.[11,33,35,47] Unlike other systems, the quantum binding is a much larger fraction of the classical binding energy, ranging from 54% for the first three molecules aggregated to EC6, down to 38% and 33% for the fourth and the fifth respectively. By contrast, H_2 is only bound by 20 wavenumbers to a water molecule,[59] or about 10% of the classical binding.

Finally, it is insightful to inspect selected radial distributions from the ground state wavefunctions. In Fig. 2 we display the Li^+ to NM distance distribution (black line) from the ground state wavefunction of EC6-$(H_2)_5$ and compare it to the Li^+ to hydrogen distance distribution for EC6-$(H_2)_5$ (red line) and for EC6-$(H_2)_4$ (blue line). The Li^+ to NM distance distribution features a single peak at 6.5 bohr and a 0.64 bohr full width at half height. The red curve is bimodal and with broader peaks. The bimodal feature of the red curve confirms the presence of two distinct types of sites, the interstitial and the surface ones. The blue curve displays a vanishingly small probability for an interstitial hydrogen molecule to be outside the octahedral cage of EC6.

3.2 EC106-$(H_2)_x$ minima Structures

The structure of the global minimum of EC106-$(H_2)_5$ is shown in Fig. 3. The one hundred THF-like Stockmayer particles are gray and are displayed as a polyhedron. The NM and hydrogen point particles are drawn with the same color scheme as in Fig. 1. The main features of the global minimum of the bare EC106,[26] are reproduced. The lithium ion is in the center of the base of a square pyramid composed of NM dipoles segregated from the THF layers. The vertex of the pyramid is oriented toward the surface of EC106. Four of the five H_2 molecules are arranged with a slightly distorted tetrahedral geometry around the Li^+ ion (brown) and partially caged between the nitromethane - like layer. One H_2 molecule is slightly above the basal plane of the square pyramid. Another molecule is on the plane, while two are below. The fifth hydrogen molecule is not visible in the figure and it is located in-

side the THF-like cluster one layer below the surface in the proximity of the NM cage. The growth pattern of the hydrogen layer

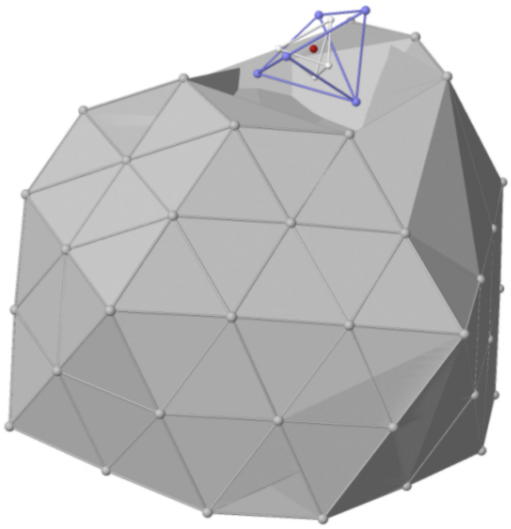

Fig. 3 The global minimum of EC106-$(H_2)_5$. The nitromethane - dipoles and hydrogen molecules are represented by blue and white spheres respectively. The lithium ion in the center of the tetrahedron is drawn as a brown sphere. Two of the four hydrogen molecules are fully caged by the Li^+ ion inside the five nitromethane - like dipoles. The sixth NM molecule and the fifth H_2 molecule are not visible in this drawing. The NM impurity is very close to the center of the THF network, whereas the fifth hydrogen is buried under the first outer layer of THF in close proximity to the NM cage.

around the lithium ion is similar to that for EC6-$(H_2)_x$. The first hydrogen molecule binds on the surface in the basal plane, the second is the farthest below the surface and behind the charge. The third occupies the surface site above the base.

cluster	V_{min} (hartree)	Classical H_2 binding (cm^{-1})
EC106	-1.020970	-
EC106-(H_2)	-1.033235	2692
EC106-$(H_2)_2$	-1.046187	2843
EC106-$(H_2)_3$	-1.057589	2502
EC106-$(H_2)_4$	-1.066482	1952
EC106-$(H_2)_5$	-1.068302	399

Table 5 Classical energies of EC106-$(H_2)_x$.

The classical minimum energy values of EC106-$(H_2)_x$ are in the second column of table 5. We find the scale of the EC101-$(H_2)_x$ systems large enough to make the estimate of the H_2 quantum chemical potential μ_x with EC106 intractable. The DMC simulations for each system requires approximately 10 kcore-hours on a modern computational grid.[60,61] The ground state energy of EC106 and its zero point energy are 0.950 hartree and 0.075 hartree respectively. These numbers have been published elsewhere.[26] However, the relative statistical fluctuations of $\langle V \rangle$ remains around one part per thousand even after combining as many as 2.4 million samples. Consequently, the binding energy of one or more hydrogen molecules, which should be comparable to those in table 4 are statistically insignificant. Nonetheless, we are able to obtain the classical estimate $\mu_x^{(c)}$, reported in column 3 of table 5, and reproducible radial distributions. These allow a semi quantitative comparison between the two sets of systems. For instance, the pattern $\mu_x^{(c)}$ is the same, and the agreement between the two sets of $\mu_x^{(c)}$ values is within 200 cm^{-1}. However, unlike in the binding pattern in EC6, the first hydrogen is on the surface and the second molecule of hydrogen is caged by the NM frame. This explains the slight increase in the binding energy of the second molecule. Therefore, while the THF layers greatly perturb the NM cage, it influences the structure and the energy of the hydrogen layer by an almost negligible extent.

3.3 EC106-$(H_2)_x$ ground state radial distributions

On the left of Fig. 4 we juxtapose the radial distribution of the Li^+ ion relative to the center of the cluster (light blue curve peaking at 22.2 bohr), with those of H_2 and D_2 (purple and green curves respectively). The breath of the distributions for H_2 and D_2 is governed mainly by the details of the PES rather than the differences in the quantum nature of the two nuclei. Nevertheless, the distribution of the D_2 molecule shows a small but significant increase in the proximity of the cation.

On the right panel of Fig. 4 we graph selected radial distributions for EC106-$(H_2)_2$. The distribution of H_2 relative to the geometric center of the cluster is bimodal with a depression near the Li^+ ion whose distribution is not shown. The two hydrogen molecules are an average of 3.5 bohr away from the Li^+ ion (green curve) and approximately 6.8 bohr away from each other (blue curve).

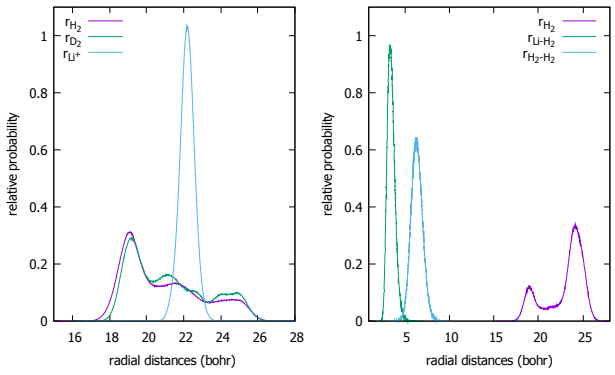

Fig. 4 Left panel: Selected radial distributions of EC106-H_2 and EC106-D_2. Right panel: Selected radial distributions of EC106-$(H_2)_2$

For the remaining three systems we graph the distance for H_2 relative to the center of EC106 in Fig. 5, the H_2 to H_2 distance in Fig. 6 and finally, the H_2 to Li^+ distance Fig. 7. The color pattern is consistent among the three figures. We use purple for $x = 3$, green for $x = 4$ and black for $x = 5$. We observe a gradual increase in the relative probability of finding hydrogen closer to the center between $n = 3$ and $n = 4$ followed by a much larger increase in deep interstitial occupancy when the fifth hydrogen molecule is

added (black curve). The same pattern can be gleaned in the remaining two distributions as peaks at larger distances from the ion and among hydrogen molecules become more visible.

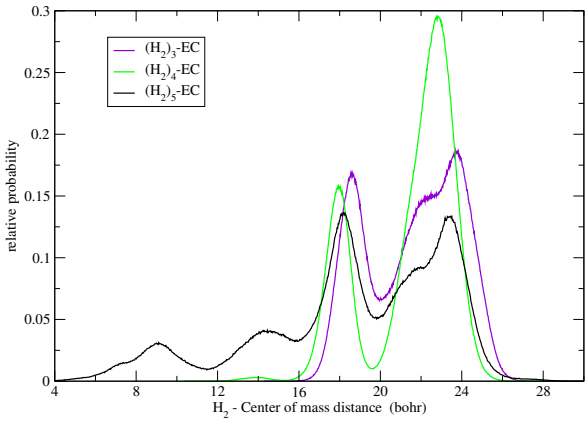

Fig. 5 Distribution of the distance of H_2 to the center of EC106 for three (purple line), four (green line), and five (black line) H_2 molecules aggregated to the electrolyte cluster.

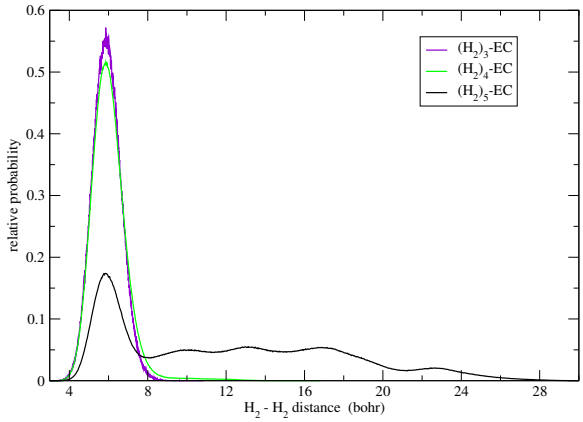

Fig. 6 Radial distribution of H_2 to H_2 for three (purple line), four (green line), and five (black line) H_2 molecules aggregated to EC106.

Perhaps, the clearest evidence that hydrogen molecules substantially perturb EC106 comes from comparing histograms of the lithium ion relative to the center, for selected systems as shown in Fig. 8. The black solid line is reproduced from Ref. 26 and is the histogram of the radial distances of Li^+ from the center of mass for EC106. Adding one molecule of hydrogen produces the red (dashed line) in the same figure. The mean and most probable value of the distance is significantly smaller in EC106-H_2, and the trend continues as the number of H_2 increases to 4. Clearly, hydrogen is drawing the lithium ion toward the bulk.

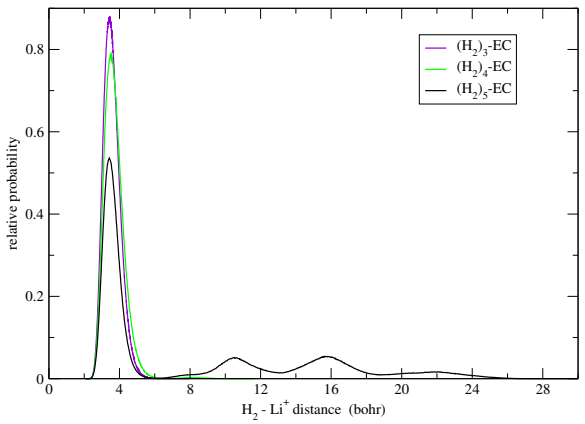

Fig. 7 Radial distribution of H_2 to Li^+ for three (purple line), four (green line), and five (black line) H_2 molecules aggregated to EC106.

4 Discussion and conclusions

When the investigation of the properties of hydrogen physisorbed by ECs began, we expected to find that the ECs framework, including the ion, could be treated as single rigid entity. We also expected to find the hydrogen bound on the surface. Instead, the simulations reveal that both these expectations, based on previous experiences with physisorbed hydrogen,[11,33,35,47] are too simplistic. In particular, the results graphed in Fig. 2 and in Fig. 4 through Fig. 8 demonstrate the complex nature of the ground state wavefunctions and most prominent features of the potential energy landscape as the hydrogen molecules are absorbed.

Our results suggest that the investigation of the ability of amorphous solids, such as frozen electrolytes and the likes, to store hydrogen deserves more attention. The storage of hydrogen caged by electrolyte clusters adds a new perspective for the field we did not anticipate. In retrospect, finding hydrogen molecules in the interstitial spaces of ECs is not a surprising result. The hydrogen molecule is much smaller than the Stockmayer particles surrounding the cation. Hydrogen is known to permeate[62] through metal, albeit via a different mechanism. Nevertheless, these results are in stark contrast with those uncovered in previous investigations of hydrogen aggregated to neutral ammonia molecules.[33–35,40,47] The lithium cation is quite small compared to the solvent dipoles, and clearly it size and charge are responsible for some of the differences we find in this study, albeit, we have sufficient evidence to expect that a neutral cluster of THF-like Stockmayer particles may cage hydrogen as well. In fact, we observe that the fifth hydrogen molecule is between solvation layers of EC106 rather than on the surface.

More investigations are needed to address a number of questions the present simulations have uncovered. To start, if we argue that electrolytic clusters are viable vectors for hydrogen storage, their size has to be optimized. What constitute such optimal size depends on the “solubility" of the ionic compound, in that, sufficient amount of “solvent" dipoles are needed to affect a

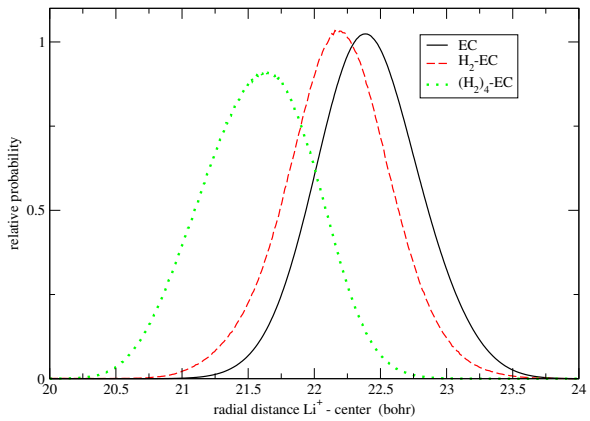

Fig. 8 Radial distribution of Li^+ relative to the cluster center for zero (black line), one (red dashed line), and four (green dotted line) H_2 aggregated molecules

meaningful separation of the charges in overall neutral bulk carrier. The potential model we use in the present investigation is perhaps best suited to provide a useful range in a tractable manner. These preliminary investigations must be followed by additional ones with other parameters, such as the dipole moment magnitude to investigate the effects of segregation vs inclusion of ions, or ion pairing etc.

Our treatment of the solvent scaffold is coarse grained and the details of the present study may not be reproduced quantitatively by a fully atomistic model with a more accurate PES. Therefore, investigations with more accurate PES models once a reasonably narrow range of sizes is identified are necessary. Improvements on the present PES should also include a treatment of the polarizations, which play an important role in the force field. It would be interesting, and certainly more feasible, to study at atomic resolution and from first principle the energies and structures of EC6-$(H_2)_x$, to see if a coordination pattern similar to Fig. 3 is observed. Depending on the actual optimum size, more advanced models could be spectroscopic precision PESs optimized from first principle electronic structure theory, or a combination of methods such as a QM / coarse-grained approach.

The fact that there are similarities between EC106-$(H_2)_x$ and EC6-$(H_2)_x$ suggests that the simulations of smaller systems may be insightful and generalizable. We anticipate the qualitative features we find for hydrogen at EC6 and EC106 to be reproduced with higher level theories. Clearly, more theoretical and experimental work is needed to verify these claims. Tagging experiments,[63,64] for example, could be used to find the number of molecules of H_2 that aggregate with a cluster like EC106. Our group is currently pursuing the development of a spectroscopically accurate hydrogen - lithium ion potential energy surface.

Acknowledgments

Acknowledgment is made to the Donors of the American Chemical Society Petroleum Research Fund, grant number ACS-PRF# 55264-UR6, for partial support of this research. This research was performed using resources provided by the Open Science Grid,[60,61] which is supported by the National Science Foundation, NSF award 1148698, and the U.S. Department of Energy's Office of Science. Arcadia University's Faculty Development Funds are also gratefully acknowledged.

5 Bibliography

Notes and references

1 *Source: Bloomburg*, `https://about.bnef.com/new-energy-outlook/`.

2 *Source: U.S. Department of Energy. n.d. Hydrogen storage challenges*, `https://www.energy.gov/eere/fuelcells/hydrogen-storage-challenges`.

3 A. Züttel, *Materials Today*, 2003, **6**, 24 – 33.

4 A. Ahmed, S. Seth, J. Purewal, A. G. Wong-Foy, M. Veenstra, A. J. Matzger and D. J. S. Siegel, *Nat Commun*, 2019, **10**, 1568.

5 G. Anderson, B. Schweitzer, R. Anderson and D. A. Gómez-Gualdrón, *The Journal of Physical Chemistry C*, 2019, **123**, 120–130.

6 V. V. Struzhkin, B. Militzer, W. L. Mao, H.-k. Mao and R. J. Hemley, *Chemical Reviews*, 2007, **107**, 4133–4151.

7 B. Zheng, R. Yun, J. Bai, Z. Lu, L. Du and Y. Li, *Inorganic Chemistry*, 2013, **52**, 2823–2829.

8 I. Cabria, M. J. López and J. A. Alonso, *The Journal of Chemical Physics*, 2008, **128**, 144704.

9 G. R. L. Dienberg, J. Haug and E. Roduner, *Phys. Chem. Chem. Phys.*, 2013, **15**, 5836–5843.

10 E. Tsivion, J. R. Long and M. Head-Gordon, *J. Am. Chem. Soc.*, 2014, **136**, 17827–17835.

11 E. Curotto and M. Mella, *The Journal of Chemical Physics*, 2018, **148**, 102315.

12 V. Buch, S. C. Silva and J. P. Devlin, *The Journal of Chemical Physics*, 1993, **99**, 2265–2268.

13 V. Buch and J. P. Devlin, *The Journal of Chemical Physics*, 1993, **98**, 4195–4206.

14 H. G. Hixson, M. J. Wojcik, M. S. Devlin, J. P. Devlin and V. Buch, *The Journal of Chemical Physics*, 1992, **97**, 753–767.

15 R. Cocco, F. Shaffer, R. Hays, S. Reddy Karri and T. Knowlton, *Powder Technology*, 2010, **203**, 3–11.

16 S.-J. Hong, H.-M. Kim, D. Huh, C. Suryanarayana and B. S. Chun, *Materials Science and Engineering: A*, 2003, **347**, 198–204.

17 K. Onuma and A. Ito, *Chemistry of Materials*, 1998, **10**, 3346–3351.

18 M. Caricato, *The Journal of Physical Chemistry C*, 2021, **125**, 27509–27519.

19 M. Z. Kamrath, R. A. Relph, T. L. Guasco, C. M. Leavitt and M. A. Johnson, *International Journal of Mass Spectrometry*, 2011, **300**, 91–98.

20 O. Gorlova, J. W. DePalma, C. T. Wolke, A. Brathwaite, T. T. Odbadrakh, K. D. Jordan, A. B. McCoy and M. A. Johnson,

The Journal of Chemical Physics, 2016, **145**, 134304.
21 B. W. Shires and C. J. Pickard, *Physical Review X*, 2021, **11**, 041026.
22 D. J. Wales and J. P. K. Doye, *J. Phys. Chem. A*, 1997, **101**, 5111–5116.
23 S.-Y. Zeng, C.-H. Hsu and T.-M. Wu, *The Journal of Physical Chemistry A*, 2022, **126**, 2018–2030.
24 D. Lu and S. J. Singer, *The Journal of Chemical Physics*, 1996, **105**, 3700.
25 D. Lu, *Ph.D. thesis*, The Ohio State University, 1996.
26 G. DiEmma, S. Kalette and E. Curotto, *Chemical Physics Letters*, 2019, **725**, 80 – 86.
27 E. Curotto, *The Journal of Chemical Physics*, 2015, **143**, 214301.
28 H. M. C. L. C. Jake and E. Curotto, *The Journal of Chemical Physics*, 2016, **144**, 174115.
29 J. B. Anderson, *The Journal of Chemical Physics*, 1975, **63**, 1499.
30 J. B. Anderson, *The Journal of Chemical Physics*, 1980, **73**, 3897.
31 D. L. M. H. Kalos and L. Verlet, *Phys. Rev. A*, 1974, **9**, 2178.
32 M. H. Kalos and P. A. Whitlock, *Monte Carlo Methods*, Wiley, New York NY, 1986.
33 M. Mella and E. Curotto, *The Journal of Chemical Physics*, 2013, **139**, 124319.
34 M. Mella and E. Curotto, *The Journal of Chemical Physics A*, 2017, **121**, 5005–5017.
35 E. Curotto and M. Mella, *The Journal of Chemical Physics*, 2017, **148**, 102315.
36 W. H. Stockmayer, *The Journal of Chemical Physics*, 1941, **9**, 398.
37 E. Curotto, *Stochastic Simulations of Clusters: Quantum Methods in Flat and Curved Spaces*, CRC, Boca Raton, FL, 2010.
38 D. L. F. E. Curotto and J. D. Doll, *The Journal of Chemical Physics*, 2008, **128**, 204107.
39 M. L. M. M. W. Avilés and E. Curotto, *The Journal of Chemical Physics*, 2008, **128**, 124517,.
40 M. M. P. E. Janeiro-Barral and E. Curotto, *J. Phys. Chem. A*, 2008, **112**, 2888.
41 M. F. R. Jr. and E. Curotto, *The Journal of Chemical Physics*, 2003, **118**, 6806.
42 J. M. F. Russo and E. Curotto, *The Journal of Chemical Physics*, 2005, **120**, 2110.
43 E. Curotto, *The Journal of Chemical Physics*, 2005, **123**, 134102.
44 P. T. G. M. W. Avilés and E. Curotto, *The Journal of Chemical Physics*, 2006, **124**, 174305.
45 S. Wolf and E. Curotto, *The Journal of Chemical Physics*, 2014, **141**, 024116.
46 S. Wolf, E. Curotto and M. Mella, *Int. J. Quantum Chem.*, 2014, **114**, 611–625.
47 E. Curotto and M. Mella, *The Journal of Chemical Physics*, 2010, **133**, 214301.
48 E. A. A.-R. M. E. C. D. L. Freeman and J. D. Doll, *The Journal of Chemical Physics*, 2009, **131**, 184508.
49 E. Curotto and M. Mella, *J.Chem.Phys.*, 2015, **142**, 114110.
50 E. Curotto and M. Mella, *J.Chem.Phys.*, 2015, **142**, 114111.
51 K. Roberts, R. Sebsebie and E. Curotto, *The Journal of Chemical Physics*, 2012, **136**, 074104.
52 A. Stringer and E. Curotto, *Chemical Physics Letters*, 2019, **734**, 136728.
53 K. Patkowski, W. Cencek, P. Jankowski, K. Szalewicz, J. B. Mehl, G. Garberoglio and A. H. Harvey, *The Journal of Chemical Physics*, 2008, **129**, 094304.
54 F. Neese, *WIREs Computational Molecular Science*, 2012, **2**, 73–78.
55 D. G. Liakos, R. Izsák, E. F. Valeev and F. Neese, *Molecular Physics*, 2013, **111**, 2653–2662.
56 F. Pavošević, P. Pinski, C. Riplinger, F. Neese and E. F. Valeev, *The Journal of Chemical Physics*, 2016, **144**, 144109.
57 T. H. Dunning, *The Journal of Chemical Physics*, 1989, **90**, 1007–1023.
58 D. E. Woon and T. H. Dunning, *The Journal of Chemical Physics*, 1994, **100**, 2975–2988.
59 P. Valiron, M. Wernli, A. Faure, L. Wiesenfeld, C. Rist, S. Kedžuch and J. Noga, *The Journal of Chemical Physics*, 2008, **129**, 134306.
60 R. Pordes, D. Petravick, B. Kramer, D. Olson, M. Livny, A. Roy, P. Avery, K. Blackburn, T. Wenaus, F. Würthwein, I. Foster, R. Gardner, M. Wilde, A. Blatecky, J. McGee and R. Quick, J. Phys. Conf. Ser., 2007, p. 012057.
61 I. Sfiligoi, D. C. Bradley, B. Holzman, P. Mhashilkar, S. Padhi and F. Wurthwein, 2009 WRI World Congress on Computer Science and Information Engineering, 2009, pp. 428–432.
62 J. Gorman and W. Nardella, *Vacuum*, 1962, **12**, 19 – 24.
63 T. K. Esser, H. Knorke, F. Siro-Brigiano, D. R. Galimberti, K. R. Asmis, M.-P. Gaigeot and J. M. Lisy, *Phys. Chem. Chem. Phys.*, 2018, **20**, 28476–28486.
64 S. Mitra, C. H. Duong, L. M. McCaslin, R. B. Gerber and M. A. Johnson, *Phys. Chem. Chem. Phys.*, 2020, **22**, 4501–4507.